

Valence and magnetism in EuPd_3S_4 and $(\text{Y}, \text{La})_x\text{Eu}_{1-x}\text{Pd}_3\text{S}_4$

D. H. Ryan

*Physics Department and Centre for the Physics of Materials, McGill University,
3600 University Street, Montreal, Quebec, H3A 2T8, Canada*

Sergey L. Bud'ko, Brinda Kuthanazhi, and Paul C. Canfield

Ames National Laboratory, and Department of Physics and Astronomy, Iowa State University, Ames, Iowa 50011, USA

(Dated: October 11, 2022)

^{151}Eu Mössbauer spectroscopy shows that yttrium substitution in mixed-valent EuPd_3S_4 drives the initial 50:50 mix of Eu^{3+} and Eu^{2+} towards pure Eu^{2+} , whereas lanthanum substitution has the opposite effect, but only for substitution levels above 50%. We find that total valence electron count and chemical pressure effects cannot account for the observed behaviour, however conserving the cell volume provides a consistent description of the changes in the $\text{Eu}^{2+}:\text{Eu}^{3+}$ ratio. Remarkably, lanthanum substitution also leads to a clear transition from static mixed-valent behavior at lower temperatures to dynamic mixed valent behavior at higher temperatures, with the onset temperature monotonically increasing with Eu content and extrapolating to a value of ~ 340 K for the pure EuPd_3S_4 compound. Magnetic order persists at least as far as $x=0.875$ in both series, despite the drastic reduction in the amount of moment-carrying Eu^{2+} ions.

I. INTRODUCTION

The rare earth palladium sulphides RPd_3S_4 have been reported for the majority of the rare earths, including yttrium¹⁻⁴. They all crystallise in the cubic NaPt_3O_4 structure ($Pm\bar{3}n$ #223) with the rare earth occupying the $2a$ site forming a bcc sublattice, the palladium on the $6d$ site and the sulphur on the $8e$ site. Remarkably, although the RPd_3S_4 phases exist for the trivalent rare earths, but apparently not for the divalent alkaline earths (Ca and Sr), when prepared with europium⁵ or ytterbium⁴ a roughly 50:50 mix of divalent and trivalent rare earth is found.

Here we will use chemical substitution of yttrium and lanthanum for europium to investigate the stability of the valence distribution and its effects on magnetic ordering. Although both ^{170}Yb and ^{151}Eu Mössbauer spectroscopy can generally be used to identify the valence of their respective target ions, for ^{170}Yb Mössbauer spectroscopy, the isomer shift between the two valence states is extremely small so the technique is almost totally dependent on the presence of an electric field gradient (efg) at the Yb^{3+} ions to identify trivalent ytterbium. Unfortunately the high symmetry of the $2a$ site makes the efg contribution effectively zero and the presence of the Yb^{3+} ions is only apparent in the magnetically ordered state well below $T_N \sim 2$ K⁴. We will therefore only study EuPd_3S_4 using ^{151}Eu Mössbauer spectroscopy where the two valence states are clearly isolated by a large difference in isomer shift, even at ambient temperatures.

We find that, by substituting Y for Eu, the remaining Eu sites become more and more divalent. In contrast, by substituting La for Eu we find that, initially, the remaining Eu sites stay roughly a 50:50 mixture of di- and tri-valent Eu, but for higher La substitution levels the remaining Eu rapidly becomes more trivalent. La substitution also leads to a transition from statically mixed valent behavior at lower temperatures to dynamically mixed

valent behavior at higher temperatures with the onset temperature (T_{onset}) monotonically increasing with Eu content and passing through room temperature as pure EuPd_3S_4 is approached. Despite the decreasing fraction of moment-carrying Eu^{2+} ions, both $\text{Y}_x\text{Eu}_{1-x}\text{Pd}_3\text{S}_4$ and $\text{La}_x\text{Eu}_{1-x}\text{Pd}_3\text{S}_4$ continue to exhibit some form of magnetic order at least as far as $x=0.875$, with transition temperatures of ~ 3 K (Y) and ~ 6 K (La).

II. EXPERIMENTAL METHODS

Polycrystalline samples of EuPd_3S_4 and $(\text{Y}, \text{La})_x\text{Eu}_{1-x}\text{Pd}_3\text{S}_4$ were prepared from stoichiometric mixtures of EuS (99.9% – American Elements) Y_2S_3 (99.9%), La_2S_3 (99%), Pd (99.95%) and S (99.5%), all from Alfa-Aesar. The powders were mixed and then pressed to form a dense pellet. This was loaded into an alumina crucible and sealed under a partial pressure of helium in a fused silica tube. The sample was heated to 650°C over three hours, held for an hour and then taken to 900°C over a further three hours. After 75 hours at 900°C the sample was furnace cooled and removed once it reached ambient temperature. In most cases this single thermal cycle was found to yield a single-phased product, however when an impurity was found (typically PdS seen by x-ray diffraction or EuS seen in susceptibility vs. temperature) the sample was crushed, pressed and subjected to a second 75 hr annealing cycle to 900°C to remove the impurity.

X-ray diffraction measurements were made on a Rigaku Miniflex-II diffractometer using a Cu-K_α source. The instrument calibration was checked using NIST 676a Al_2O_3 and found to be consistent within fitted uncertainties. Full Rietveld refinement of the diffraction patterns was carried out using the GSAS/EXPGUI packages^{6,7}. As all three species occupy special sites in the $Pm\bar{3}n$ structure, no positional parameters were adjusted dur-

ing the fits. For the yttrium and lanthanum substituted samples only random occupation of the Eu(2a) site was considered.

^{151}Eu Mössbauer spectroscopy measurements were carried out using a 4 GBq $^{151}\text{SmF}_3$ source, driven in sinusoidal mode. The drive motion was calibrated using a standard $^{57}\text{CoRh}/\alpha\text{-Fe}$ foil. Isomer shifts are quoted relative to EuF_3 at ambient temperature. The 21.6 keV gamma rays were recorded using a thin NaI scintillation detector. For temperatures above 5 K, the samples were cooled in a vibration-isolated closed-cycle helium refrigerator with the sample in a helium exchange gas. Temperatures below 5 K were achieved using a helium flow cryostat while pumping on the sample space and using a needle valve to throttle the flow. The spectra were fitted to a sum of Lorentzian lines with the positions and intensities derived from a full solution to the nuclear Hamiltonian⁸.

Temperature- and magnetic field- dependent magnetization measurements ($1.8\text{ K} \leq T \leq 300\text{ K}$, $0\text{ T} \leq \mu_0 H \leq 7\text{ T}$) were performed using a Quantum Design MPMS-3 SQUID magnetometer. The sample was confined in a #4 gelatin capsule and a transparent drinking straw was used as a sample holder. Low-temperature heat capacity measurements were made using semiadiabatic thermal relaxation technique as implemented in the heat capacity option of a Quantum Design Physical Property Measurement System (PPMS). For selected samples, the ^3He option was used to cool to $\sim 0.4\text{ K}$. Sintered samples of 20–70 mg mass with at least one flat surface were mounted on a micro-calorimeter platform using Apiezon N grease. The addenda (platform + grease) heat capacity was measured separately for each sample and subtracted from the total heat capacity using the PPMS software. Although the samples possibly had reduced density, the measured sample coupling parameter took reasonable values of more than 97%.

III. RESULTS

A. EuPd_3S_4

Fitting the x-ray diffraction pattern of the EuPd_3S_4 sample showed it to be single phased with the expected cubic NaPt_3O_4 structure² and a lattice parameter of $a = 6.6786(1)\text{ \AA}$ (Fig. 1). The room temperature ^{151}Eu Mössbauer spectrum showed two distinct contributions from Eu^{3+} and Eu^{2+} in the ratio 50.4(4):49.6(4), with the linewidth of the Eu^{2+} component being slightly broader, in complete agreement with previous reports⁵. On cooling to 5 K the ratio becomes 46.2(5):53.8(5) (Fig. 2) as the Debye temperature of the Eu^{3+} component is slightly higher than that of the Eu^{2+} component. Fitting the temperature dependence of the two component areas to a simple Debye model, as shown in Fig. 3, yields Debye temperatures of 227(3) K (Eu^{3+}) and 204(3) K (Eu^{2+}). It is important to emphasise that any *apparent* changes in

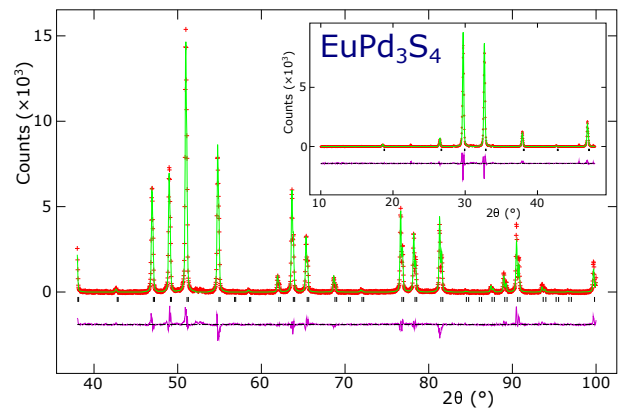


FIG. 1. Cu- K_α x-ray diffraction pattern for EuPd_3S_4 . Solid line is a full Rietveld refinement using the GSAS/EXPGUI packages^{6,7}. The line below the data shows the residuals. Tick marks between the data and residual lines show the calculated positions of the Bragg peaks. The inset shows the low-angle range. The diffraction pattern was collected in two overlapping blocks with a longer counting time at higher angles to compensate for the loss of intensity due to the effects of the x-ray form factor.

the $\text{Eu}^{2+}:\text{Eu}^{3+}$ ratio with temperature in Fig. 3 do not reflect *actual* changes in the ratio, rather they are the result of the different temperature dependences of the recoil-free-fractions (often denoted f) for the two species. In order to minimise the impacts of this effect, all valence ratios will be taken from low-temperature spectra.

On cooling to 1.8 K, the Eu^{2+} component develops a clear magnetic splitting whereas the Eu^{3+} component is unchanged, consistent with trivalent europium being non-magnetic (Fig. 2). In principle one might anticipate a small transferred field at the Eu^{3+} sites from the ordered Eu^{2+} moments, however none was observed and no increase in the width of the Eu^{3+} component was detected ($B_{hf} \ll 1\text{ T}$), perhaps as a result of cancellations arising from the antiferromagnetic ordering of the Eu^{2+} moments. The hyperfine field (B_{hf}) for the Eu^{2+} component at 1.8 K is 29.9(2) T, typical for ordered Eu^{2+} , and fitting the temperature dependence shown in Fig. 4 to the expected $J = \frac{7}{2}$ Brillouin function yields a $T=0$ $B_{hf}=37.9(6)\text{ T}$ and an ordering temperature of $T_N=2.90(1)\text{ K}$ in good agreement with both previous work⁵ and our own susceptibility and C_p data (Fig. 5). The clear cusp in the susceptibility *vs.* temperature is consistent with antiferromagnetic (AF) ordering and it is accompanied by a sharp peak in the heat capacity. The high-field magnetisation curve taken at 1.8 K (inset to Fig. 5) shows that the system is readily saturated despite the AF order, consistent with the low ordering temperature as well as the low anisotropy typically associated with the Eu^{2+} ion. Furthermore, the maximum moment observed in the applied field of 7 T suggests a Eu^{2+} fraction of 50% (assuming a moment of $7\text{ }\mu_B/\text{Eu}^{2+}$) consistent with the 53.8(5)% derived above from the ^{151}Eu Mössbauer spectrum at 5 K, and with earlier results^{5,9}.

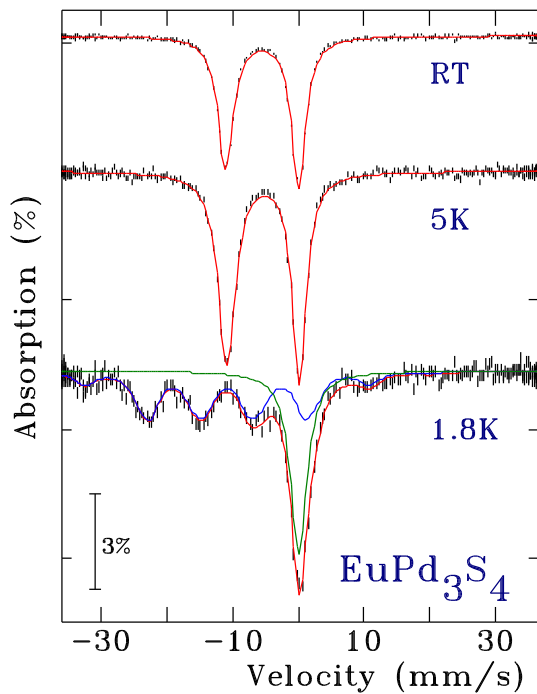


FIG. 2. ^{151}Eu Mössbauer spectra of EuPd_3S_4 at RT (top), 5 K (middle), and 1.8 K (bottom). Between RT and 5 K the primary changes are a significant increase in the absorption due to conventional thermal effects and a slight change in the 2+:3+ area ratio due to differences in the Debye temperatures of the two components. At 5 K the two valence contributions are almost equal in area and fully resolved, with the Eu^{2+} at $-10.91(2)$ mm/s and Eu^{3+} at $+0.07(1)$ mm/s. At 1.8 K only the Eu^{2+} component is ordered and shows a hyperfine field (B_{hf}) of $29.9(2)$ T, while the Eu^{3+} component is unchanged. The solid red lines are fits as described in the text. For the 1.8 K spectrum we also show the magnetically split Eu^{2+} and unchanged Eu^{3+} components.

The unusual and apparently stable valence mix in EuPd_3S_4 leads to the question: “why?”. What makes europium (and ytterbium) “special”? How robust is the valence distribution? Can we change it?

As the Eu^{3+} ion is smaller than the Eu^{2+} ion, one might expect hydrostatic pressure to promote $\text{Eu}^{2+} \rightarrow \text{Eu}^{3+}$ conversion. Alternatively, if we force some fraction of the R sites to be unambiguously trivalent, by replacing some of the europium with a formally trivalent ion, will this cause more of the remaining europium to become divalent to preserve the average electron count?

Although the driving that can be achieved by chemical substitution is not as clean as that generated by direct hydrostatic pressure, it is much easier to make direct measurements of the valence distribution, magnetisation and transition temperatures in doped samples at ambient pressures. We turn therefore to an investigation of the impacts of chemical substitution on EuPd_3S_4 using the non-moment bearing, trivalent La and Y ions with $r_{ionic}(\text{Eu}^{2+}) \gtrsim r_{ionic}(\text{La}^{3+}) > r_{ionic}(\text{Eu}^{3+}) > r_{ionic}(\text{Y}^{3+})$. If, on the one hand, the total valence elec-

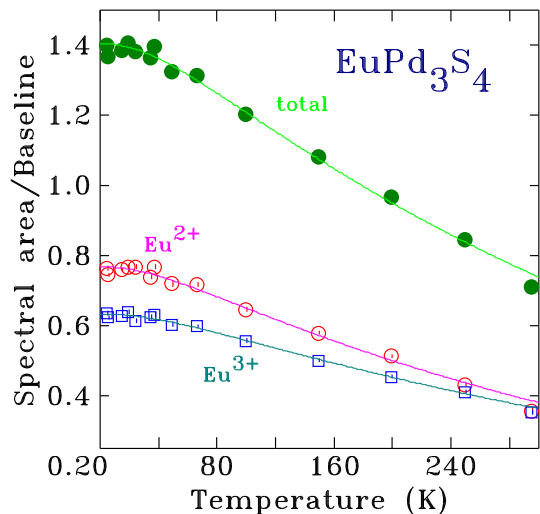


FIG. 3. Temperature dependence of the normalised (adjusted for total counting time) area of both the total spectrum and the two valence components in the ^{151}Eu Mössbauer spectra of EuPd_3S_4 . Solid lines in each case are fits to a simple Debye model yielding Debye temperatures of $227(3)$ K (Eu^{3+}) and $204(3)$ K (Eu^{2+}). Fitting the total spectral area yields an average Debye temperature of $212(3)$ K.

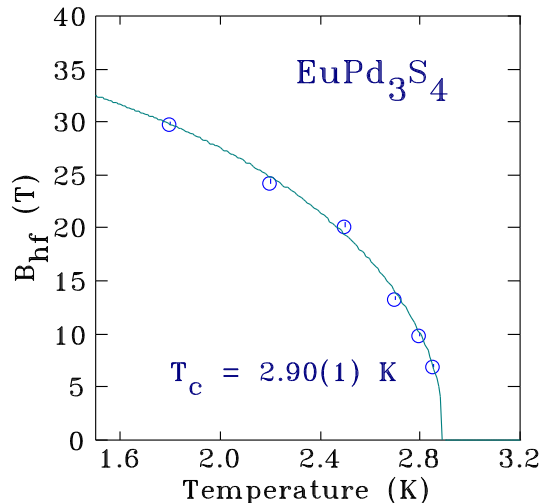


FIG. 4. Temperature dependence of hyperfine field (B_{hf}) for EuPd_3S_4 fitted using the expected $J = \frac{7}{2}$ Brillouin function to obtain the ordering temperature of $T_N = 2.90(1)$ K.

tron count is a dominant factor, then partially replacing the europium with an unambiguously trivalent ion should lead to a compensating increase in the Eu^{2+} fraction. On the other hand, if preserving the cell volume is critical, then the lattice expansion that would be caused by introducing the $r_{ionic}(\text{La}^{3+}) \lesssim r_{ionic}(\text{Eu}^{2+})$ lanthanum ion could be compensated by some $\text{Eu}^{2+} \rightarrow \text{Eu}^{3+}$ conversion (the reverse being expected for the $r_{ionic}(\text{Y}^{3+}) < r_{ionic}(\text{Eu}^{3+})$ yttrium ion). Alternatively, if the substitutions act as chemical pressures, then expanding the cell using lanthanum substitution should lead to

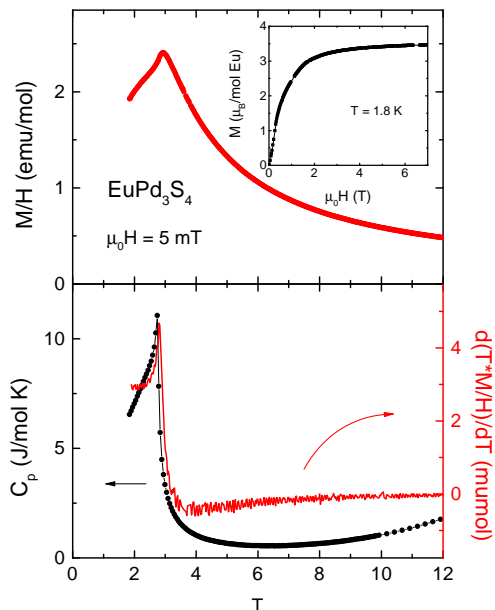


FIG. 5. Top: DC susceptibility vs. temperature for EuPd_3S_4 showing a cusp at $T_N \sim 3$ K. Inset shows M vs. $\mu_0 H$ at 1.8 K confirming that half of the europium is divalent. Bottom: Temperature dependence of the heat capacity (black points) revealing the corresponding cusp associated with the AF transition, with $d(T \cdot M/H)/dT$ (red line) showing that $C_p(T)$ and the temperature derivative of $T \cdot M/H$ take the same form around the transition.

$\text{Eu}^{3+} \rightarrow \text{Eu}^{2+}$ conversion (again, the reverse process being expected for yttrium substitution). As we show below, we can clearly distinguish between these three options.

B. Valence impacts

Fitting the x-ray diffraction data for the yttrium and lanthanum substituted compounds showed that they all retained the expected NaPt_3O_4 structure but with progressively smaller (Y) or larger (La) lattice parameters (Fig. 6). There is a clear, and significant, change in lattice parameters for both Y and La substitution. We detect no indication of phase separation in the powder x-ray diffraction data, *i.e.* no broadening or splitting of peaks that would suggest segregation of the samples into Eu-rich and Eu-poorer phases.

For the Y-substituted series, the fitted lattice parameters all lie visibly above the line connecting the Eu and Y compounds, suggesting that a shift towards more of the larger Eu^{2+} ion occurs, as the yttrium content is increased. This valence shift is confirmed directly by the 5 K ^{151}Eu Mössbauer spectra shown in Fig. 7, where the line near 0 mm/s associated with the trivalent europium decreases rapidly in intensity as the level

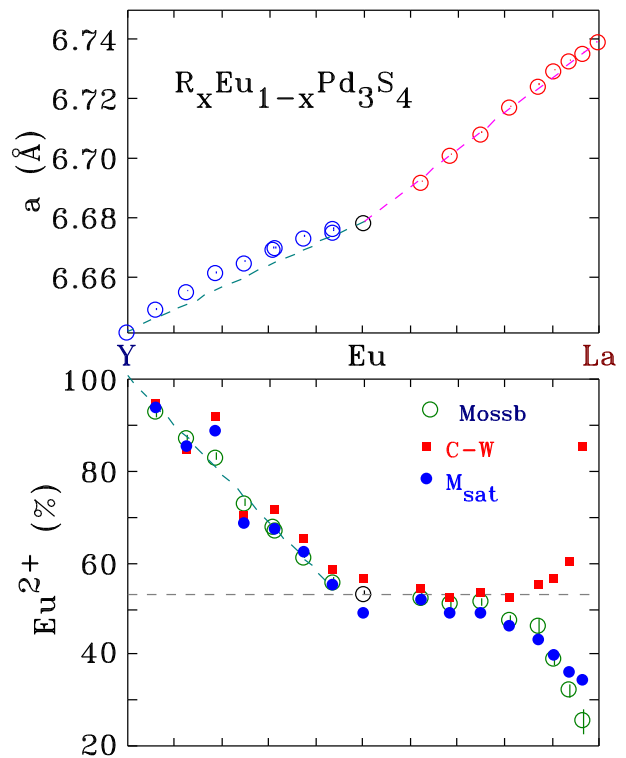


FIG. 6. (top) Lattice parameters for $(\text{Y,La})_x\text{Eu}_{1-x}\text{Pd}_3\text{S}_4$ showing the expansion associated with La-substitution and the contraction when yttrium is substituted. We note that whereas the values for the La-substituted series lie on the line connecting the pure La and Eu compounds, those for the Y-substituted samples lie significantly above the corresponding line between the pure Eu and Y compounds. (bottom) The Eu^{2+} fractions in the pure and Y,La-substituted compounds showing that Y-substitution leads to a significant shift towards more Eu^{2+} , while La-substitution initially appears to have no effect, but for $x > 0.5$ there is a marked shift towards Eu^{3+} . Open circles show values taken from ^{151}Eu Mössbauer spectroscopy at 5 K (Y-substituted) or 10 K (La-substituted); solid symbols show values derived from bulk magnetisation data: high-temperature Curie-Weiss fits (red squares), saturation magnetisation (blue circles). The deviation of the Curie-Weiss values for the La-rich compounds reflects the development of dynamic effects discussed in the text.

of yttrium substitution increases. (All valence ratios for the Y-substituted series were taken from 5 K spectra to minimise the impacts of f -factor differences for the two species, as noted above.) Both magnetisation measurements in the ordered state at 1.8 K (Fig. 8) and Curie-Weiss fits to the temperature dependence of the susceptibility above 10 K, further support these observations (see below). The Eu^{2+} fractions derived from all three measurements are summarised in the lower panel of Fig. 6.

By contrast with the yttrium-substituted series, the effects of lanthanum substitution are more complex and nuanced. The lattice parameters of the La-substituted compounds lie much closer to the line connecting the two end

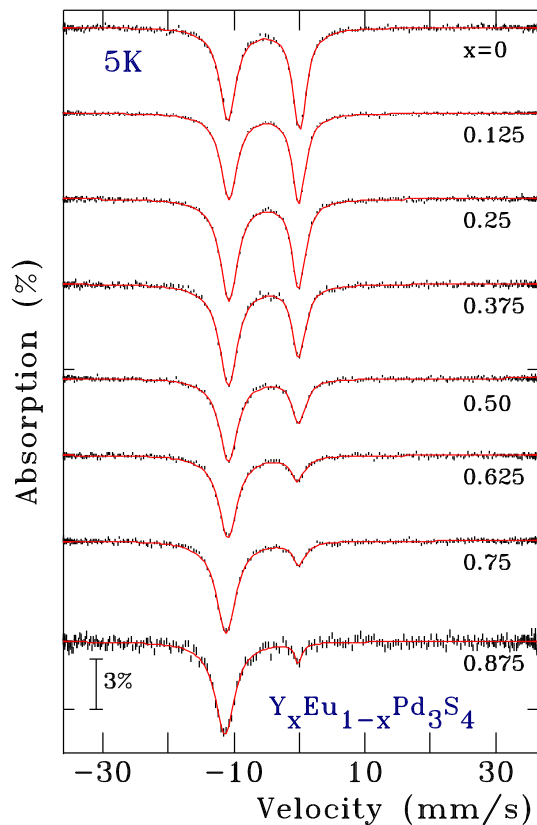


FIG. 7. ^{151}Eu Mössbauer spectra of $\text{Y}_x\text{Eu}_{1-x}\text{Pd}_3\text{S}_4$ at 5 K showing the loss of the Eu^{3+} component (the line at ~ 0 mm/s) as the level of yttrium substitution increases. The spectrum for $x=0.875$ has been rescaled by a factor of 2.5 to compensate for the low Eu content.

members (upper panel of Fig. 6) for all substitution levels, and the Eu^{2+} fraction derived from ^{151}Eu Mössbauer spectroscopy at 10 K (Fig. 9) is essentially constant (lower panel of Fig. 6) for $x \leq 0.5$. This is consistent with the fact that $r_{\text{ionic}}(\text{Eu}^{2+}) \gtrsim r_{\text{ionic}}(\text{La}^{3+}) > r_{\text{ionic}}(\text{Eu}^{3+})$ and initial La substitution does not force any significant change in the $\text{Eu}^{2+}:\text{Eu}^{3+}$ ratio. However, once about half of the europium has been replaced by lanthanum, further substitution leads to a marked change in behaviour, again consistent with the fact that $r_{\text{ionic}}(\text{La}^{3+})$ is ultimately somewhat closer to $r_{\text{ionic}}(\text{Eu}^{2+})$ rather than $r_{\text{ionic}}(\text{Eu}^{3+})$. It is readily apparent from Fig. 9 that the line near -11 mm/s that corresponds to Eu^{2+} decreases in relative intensity and this rapid loss of the divalent fraction is confirmed by the magnetisation measurements shown in Fig. 10. We use 10 K Mössbauer data for the La-substituted series, rather than the 5 K data as was used for the Y-substituted series, to avoid complications due to the onset of magnetic ordering (see below).

Finally, as is clear in Fig. 6, the Eu^{2+} fraction derived from Curie-Weiss fits (data shown below) to the temperature dependence of the susceptibility, for $\text{La}_x\text{Eu}_{1-x}\text{Pd}_3\text{S}_4$ with $x \gg 0.5$ (measured on the same sample as part of the run used to obtain the saturation magnetisation) appears

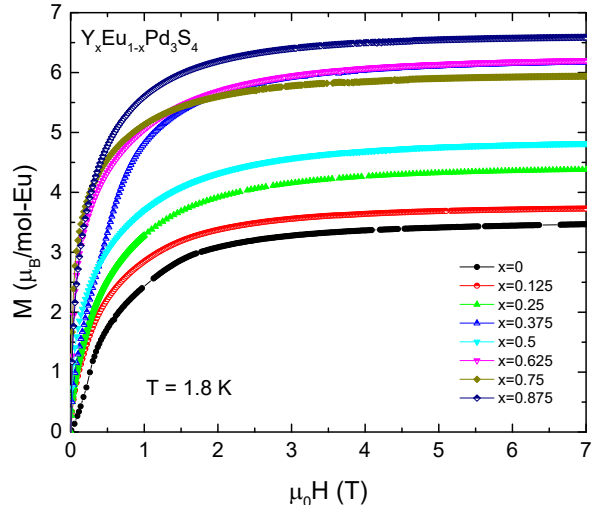


FIG. 8. High-field magnetisation curves measured at 1.8 K for $\text{Y}_x\text{Eu}_{1-x}\text{Pd}_3\text{S}_4$ showing the increase in moment/mol-Eu with increasing yttrium content as the substitution promotes $\text{Eu}^{3+} \rightarrow \text{Eu}^{2+}$ conversion. All of the curves appear to saturate in about 3–4 T, reflecting the low anisotropy associated with the Eu^{2+} ion.

to show the *opposite* behaviour – a marked *growth* in the effective moment and hence the derived Eu^{2+} fraction. As we show below, this is most likely due to dynamic effects that lead to intermediate valence behaviour of the europium ions and makes a simple Curie-Weiss analysis intractable over the temperature range available to us.

C. Dynamics in the Yttrium and Lanthanum substituted series

We have presented low-temperature Mössbauer data for the yttrium- (5 K) and lanthanum- (10 K) substituted series in order to minimise the impacts of the differing Debye temperatures of the two valence components in the spectra. Figures 11 and 12 present the room temperature Mössbauer spectra for the $\text{Y}_x\text{Eu}_{1-x}\text{Pd}_3\text{S}_4$ and $\text{La}_x\text{Eu}_{1-x}\text{Pd}_3\text{S}_4$ series. As can be seen, the differences between the room temperature and 5 K yttrium data are minimal and certainly not qualitative. However, for the $\text{La}_x\text{Eu}_{1-x}\text{Pd}_3\text{S}_4$ series, the changes in the spectra on warming go far beyond the simple, and expected, slight reduction in the apparent Eu^{2+} fraction with increasing temperature. As is clear from the RT spectra of $\text{La}_x\text{Eu}_{1-x}\text{Pd}_3\text{S}_4$ shown in Fig. 12, an entirely new feature appears in the spectra and eventually dominates the pattern by $x=0.875$. This feature is a line located midway between the lines associated with Eu^{2+} and Eu^{3+} . As Fig. 13 shows, the position of this line is essentially composition independent, appearing for all compositions $0.25 \leq x < 1.00$, and lying almost precisely midway between

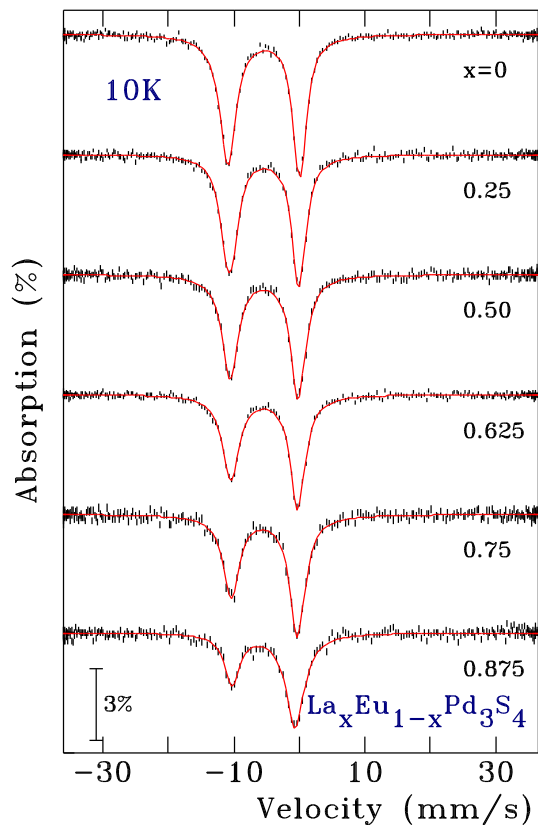


FIG. 9. ^{151}Eu Mössbauer spectra of $\text{La}_x\text{Eu}_{1-x}\text{Pd}_3\text{S}_4$ at 10 K showing an essentially constant $\text{Eu}^{2+}:\text{Eu}^{3+}$ distribution up to $x=0.50$ followed by a marked drop in the Eu^{2+} fraction above that point. Spectra taken at 10 K are used here to avoid complications associated with the magnetic ordering of the Eu^{2+} component at 6 K.

the Eu^{2+} and Eu^{3+} lines, leading us to identify it as being due to intermediate-valence europium: “ $\text{Eu}^{2.5+}$ ”. In many other intermediate-valence europium compounds such as EuCu_2Si_2 ^{10,11} and EuPd_2Si_2 ¹², where the electron exchange is between the europium and the conduction band,^{13,14} the isomer shift of the intermediate valence component is strongly temperature dependent¹⁰ as electrons initially associated with the Eu^{2+} ions spend more time in the conduction band so that the average europium valence (and hence isomer shift) changes. That is not the case here as the electron exchange is between Eu^{2+} and Eu^{3+} ions, and as long as the residence time on each ion is roughly the same, then the time-averaged valence is constant, even if the residence time (or equivalently, the hopping rate) changes.

The area of the intermediate valence feature is strongly dependent on both temperature and composition (Fig. 14). At base temperature the area of the intermediate valence feature is zero, but as temperature increases beyond T_{onset} it starts to increase, with T_{onset} decreasing with increasing x , *i.e.* increasing with increasing Eu concentration. Fig 15 plots T_{onset} versus x ; the extrapolation of the data to $x=0$, *i.e.* pure EuPd_3S_4 ,

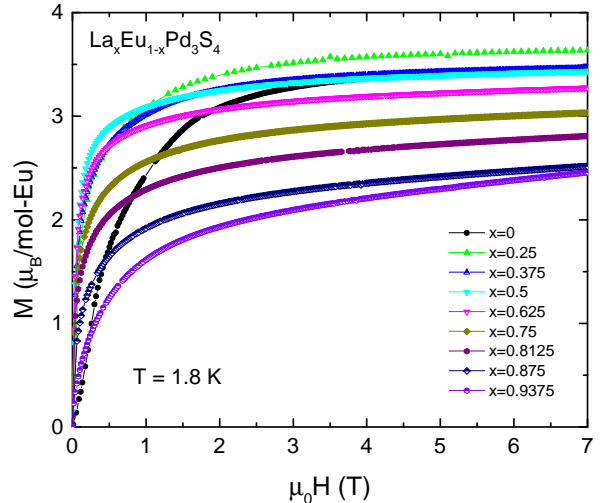


FIG. 10. High-field magnetisation curves measured at 1.8 K for $\text{La}_x\text{Eu}_{1-x}\text{Pd}_3\text{S}_4$ showing an approximately constant moment/mol-Eu with increasing lanthanum content up to $x = 0.5$ as the $\text{Eu}^{2+}:\text{Eu}^{3+}$ ratio remains largely independent of the lanthanum content, then there is a marked drop as rapid $\text{Eu}^{2+} \rightarrow \text{Eu}^{3+}$ occurs.

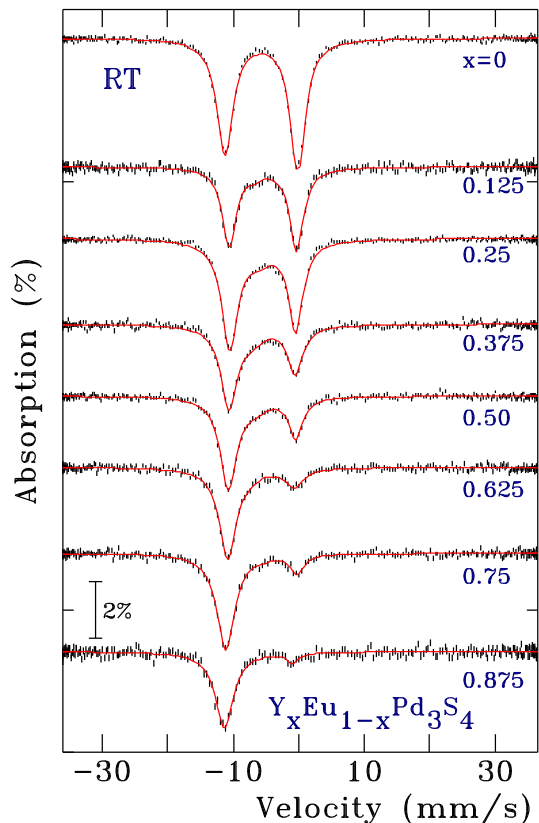


FIG. 11. Room temperature ^{151}Eu Mössbauer spectra of $\text{Y}_x\text{Eu}_{1-x}\text{Pd}_3\text{S}_4$ showing minimal changes from the 5 K spectra shown in Fig. 7 beyond the expected impacts of the differing Debye temperatures of the two valence components.

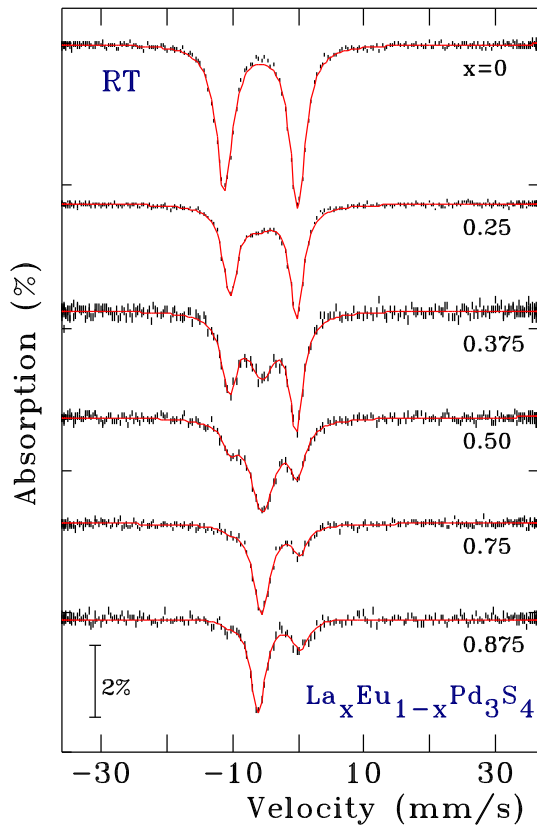


FIG. 12. Room temperature ^{151}Eu Mössbauer spectra of $\text{La}_x\text{Eu}_{1-x}\text{Pd}_3\text{S}_4$ showing the development of a new, intermediate valence feature with increasing lanthanum content.

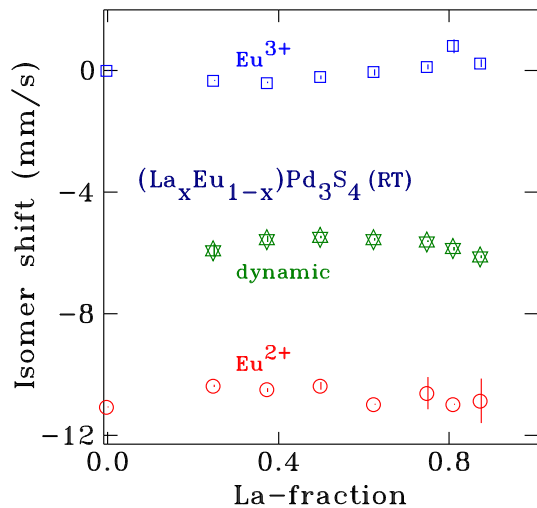


FIG. 13. Isomer shifts of the three components seen in the RT ^{151}Eu Mössbauer spectra of $\text{La}_x\text{Eu}_{1-x}\text{Pd}_3\text{S}_4$ (shown in Fig. 12) showing that the values are relatively constant for all three, and that the dynamic, intermediate valence component lies between the Eu^{2+} and Eu^{3+} component, suggesting a composition-independent valence of $\sim\text{Eu}^{2.5+}$.

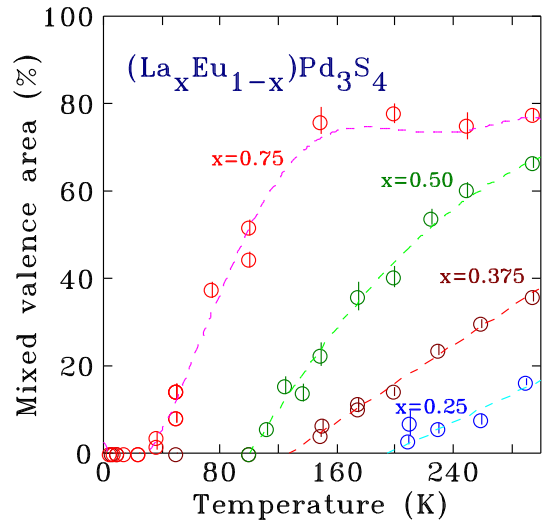


FIG. 14. Temperature dependence of the fitted area of the intermediate valence feature for $\text{La}_x\text{Eu}_{1-x}\text{Pd}_3\text{S}_4$ showing both the greater extent and earlier onset associated with increasing lanthanum substitution. Dashed lines are guides to the eye.

suggests that T_{onset} should occur near $T \sim 340$ K. The inset to Fig 15 shows the intermediate valence area data presented in Fig. 14, plotted versus effective temperature, T/T_{onset} . The data scale well and this suggests that temperatures well above 340 K will need to be measured for pure EuPd_3S_4 in order to see the intermediate valence signal. The progressive decrease in T_{onset} apparent in Fig 15 for the La-substituted series suggests that lanthanum substitution reduces the barrier for electron hopping in $\text{La}_x\text{Eu}_{1-x}\text{Pd}_3\text{S}_4$.

Finally, although the position of the $\text{Eu}^{2.5+}$ line appears to be both composition and temperature independent, its width is not. As is clear from Fig. 16, the $\text{Eu}^{2.5+}$ line becomes progressively sharper with increasing temperature while the widths of the Eu^{2+} and Eu^{3+} lines remain unchanged. This sharpening is characteristic of motional narrowing.

Thermally driven conversion of Eu^{2+} and Eu^{3+} to an average $\text{Eu}^{2.5+}$ is consistent with rapid electron hopping between the two species. Clearly, the two valence states are equally stable in EuPd_3S_4 and in the absence of evidence for charge ordering, it would appear that the spatial distribution of the two species on the 2a site is essentially random. If a given site is randomly $2+$ or $3+$, there would appear to be no reason to expect that selection to be time-independent, and given sufficient thermal energy an electron might be expected to jump from a Eu^{2+} site to a neighbouring Eu^{3+} site, exchanging the valence of the two sites in the process. If the residence time of the electron is much longer than the characteristic measuring time used to detect the valence (~ 10 – 100 ns for Mössbauer spectroscopy) then the system appears static and two distinct valence states are seen. If the residence time is much shorter, then an averaged valence is seen. Intermediate residence times (“slow re-

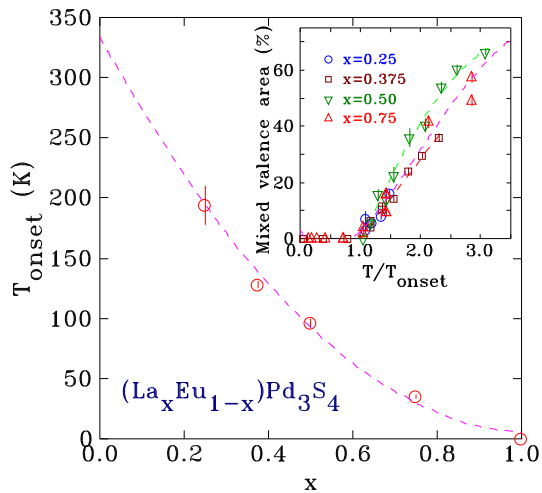


FIG. 15. Composition dependence of the temperature at which the intermediate valence feature first appears in the ^{151}Eu Mössbauer spectra of $\text{La}_x\text{Eu}_{1-x}\text{Pd}_3\text{S}_4$ (see Fig. 14). The dashed line is a guide to the eye showing an extrapolation to $x=0$ that suggests a similar transition for pure EuPd_3S_4 near 340 K. The inset shows how the composition and temperature dependences from Fig. 14 collapse when scaled to T_{onset} .

laxation”) can lead to more complex behaviour in the spectrum, but in the current case where the two components are single lines with no significant quadrupole or magnetic splittings, slow relaxation simply leads to a broad dynamic component. Raising the temperature generally leads to faster hopping and a shorter residence time and the system evolves from fully static, through the slow relaxation regime, to dynamically averaged (or motionally narrowed). As can be seen for $x=0.75$ in Fig. 14, a weak broad line appears, it becomes stronger and sharper (Fig. 16) as more europium sites become dynamic and motional narrowing occurs, finally developing into a natural-width line as the hopping rate increases and moves up out of the Mössbauer window.

It is likely that the $\text{Eu}^{2+}/\text{Eu}^{3+}$ dynamics and the development of intermediate valence europium are the cause of the difference between the estimate of percentage of Eu^{2+} between the Mössbauer, $M(H)$ and $M(T)$ data for the lanthanum substituted samples shown in Fig. 6. The ^{151}Eu Mössbauer and the saturation magnetisation measurements were made at 10 K and 1.8 K respectively, well below T_{onset} , and the valence ratios derived from them are in agreement. However, the Curie-Weiss analysis relies on measurements made at much higher temperature ranges where the intermediate valence behaviour is both pronounced and temperature dependent. Indeed, as the intermediate valence fraction becomes larger (Fig. 14), the Curie-Weiss-derived Eu^{2+} fraction deviates more strongly from the Mössbauer and saturation magnetisation values (Fig. 6). A simple Curie-Weiss analysis of temperature-dependent susceptibility is not valid where the valence and hence europium moment

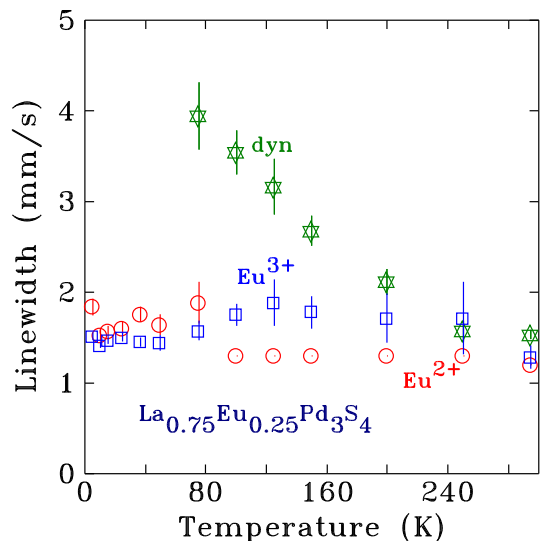


FIG. 16. Temperature dependence of the spectral linewidths for the three components seen in the ^{151}Eu Mössbauer spectra of $\text{La}_{0.75}\text{Eu}_{0.25}\text{Pd}_3\text{S}_4$. The Eu^{2+} and Eu^{3+} features have constant linewidths, as expected. However, the dynamic feature associated with the appearance of the $\text{Eu}^{2.5+}$ component clearly sharpens with increasing temperature reflecting motional narrowing associated with an increasing relaxation rate.

is strongly temperature dependent.

Finally, we note that if the same intermediate valence behaviour is present in $\text{Y}_x\text{Eu}_{1-x}\text{Pd}_3\text{S}_4$ at RT it accounts for less than 10% of the total area (Fig. 11). The difference between the yttrium- and lanthanum-substituted series may reflect stabilisation of Eu^{2+} by yttrium substitution, but there is also a very rapid loss of Eu^{3+} as yttrium is added, so as we approach the substitution levels where the $\text{Eu}^{2.5+}$ component dominated in $\text{La}_x\text{Eu}_{1-x}\text{Pd}_3\text{S}_4$, there is almost no Eu^{3+} left in $\text{Y}_x\text{Eu}_{1-x}\text{Pd}_3\text{S}_4$ to exchange electrons with the majority Eu^{2+} , so the absence of intermediate valence europium may simply be the result of limited supply.

D. Magnetic ordering

Although the Eu^{2+} fraction does increase as yttrium is added, there is a steady decline in the net moment-bearing rare-earth content of the $\text{Y}_x\text{Eu}_{1-x}\text{Pd}_3\text{S}_4$ series with increasing x . This decline is even stronger in the $\text{La}_x\text{Eu}_{1-x}\text{Pd}_3\text{S}_4$ series as the Eu^{2+} fraction is either constant (up to $x\sim 0.5$) or decreases with increasing x . Despite these monotonic reductions in the moment-bearing fraction, Fig. 17 shows that both series continue to exhibit some form of magnetic order, at least as far as $x=0.875$. Furthermore, it is apparent from both the high-field magnetisation curves (Figs. 8 and 10) and low-field dc susceptibility (Figs. A.2 and A.4 in the appendix) that both series develop some ferromagnetic character to

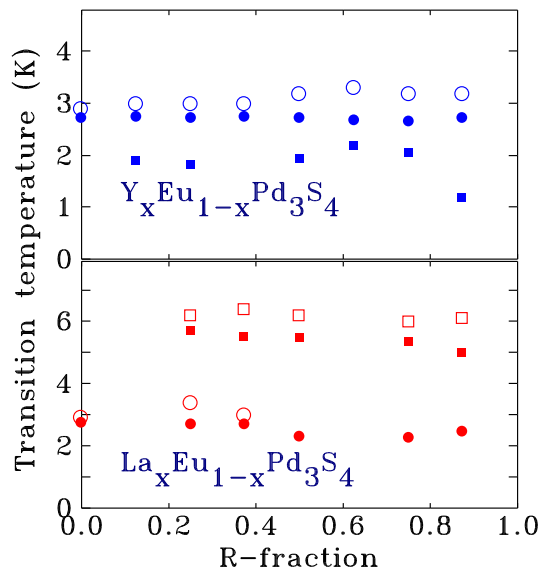


FIG. 17. Estimated transition temperatures for (top) $Y_xEu_{1-x}Pd_3S_4$ and (bottom) $La_xEu_{1-x}Pd_3S_4$. Open symbols show estimates derived from dc susceptibility while solid symbols are based on C_p data.

their ordering. Heat capacity measurements (Figs. A.1 and A.3 in the appendix) confirm the persistence of magnetic ordering. With increasing dilution, the signature of the ordering becomes progressively weaker, with a softer onset, but it is never lost.

For $Y_xEu_{1-x}Pd_3S_4$ the onset of magnetic order appears to be largely insensitive to the level of substitution, remaining near 3 K for all x . However the Y-substituted samples also exhibit a secondary feature around 2 K in the heat capacity data, and it too is largely independent of the composition.

For $La_xEu_{1-x}Pd_3S_4$, heat capacity (Fig. A.3 in the appendix) and dc susceptibility (Fig. A.4 in the appendix) measurements show that the ordering behaviour is more complex in the lanthanum substituted series. Whereas the ~ 3 K feature from the parent compound persists for all finite x , but becomes progressively less distinct, a new feature develops at ~ 6 K as lanthanum is added. This is despite the steady dilution of the moment bearing component: by $x=0.875$ only $\sim 4\%$ of the rare earth atoms are moment-bearing Eu^{2+} , yet the 6 K magnetic feature is still apparent in both heat capacity and susceptibility. ^{151}Eu Mössbauer spectroscopy confirms that the 6 K feature at $x=0.75$ is indeed magnetic and associated with the Eu^{2+} in the material. Although the ~ 5 K limit of the closed-cycle fridge was not low enough to yield a fully resolved magnetic splitting, Fig. A.5 (in the appendix) shows that it is possible to observe the initial line broadening that occurs as order develops. Fitting the broad Eu^{2+} line at 5.3 K yields a hyperfine field of 11(1) T. Fig. 17 summarises the composition dependence of the transition temperatures observed for $(Y, La)_xEu_{1-x}Pd_3S_4$.

The form of $C_p(T)$ for $La_{0.25}Eu_{0.75}Pd_3S_4$, and to a lesser extent $La_{0.375}Eu_{0.625}Pd_3S_4$, might lead one to suspect that either an impurity phase is present, or that the sample has perhaps separated into La-rich and La-poor regions, yielding distinct ~ 6 K and ~ 3 K transitions respectively. The magnitude of the C_p signal would require a rather significant impurity content to account for it. None was detected by x-ray diffraction, as noted earlier. Furthermore, the change in lattice parameter with x in the La-substituted series is quite strong (see Fig. 6) so any phase separation would yield broadened, or more likely split, diffraction lines. These were not seen in any sample studied here. Finally, the $NaPt_3O_4$ form of RPd_3S_4 appears to be stable across the entire rare-earth series and for both the Y- and La- substituted series studied here, giving us no reason to expect phase separation. The monotonic composition and temperature evolution of the intermediate valence component apparent in Figs. 12 and 14 also argues for homogeneous, rather than phase separated samples. The ^{151}Eu Mössbauer spectra in Fig. A.6 (in the appendix) reveal a progressive development of magnetic order on cooling: The Eu^{2+} component near -11 mm/s first broadens below 6 K, then a full magnetic pattern appears (more apparent on the low-velocity side of the Eu^{2+} component) on further cooling. Even at 1.8 K the magnetic component is extremely broad (compare the 1.8 K spectrum in Fig. A.6 (in the appendix) with that of $EuPd_3S_4$ at the same temperature in Fig. 2). A simple parametrisation of the spectra was obtained by using three components to fit the Eu^{2+} contribution: zero field, low-field and high-field. Fewer components gave a poor fit while using more led to instabilities. Following the areas of the magnetic and non-magnetic Eu^{2+} components (Fig. A.7 in the appendix) shows a gradual shift from non-magnetic to magnetic starting below 6 K with no apparent break near 3 K. The average magnetic field shown in Fig. A.8 (in the appendix) shows similar behaviour, again with no break near 3 K. We conclude that although the Eu^{2+} experiences a very broad range of magnetic environments, there is no evidence for phase separation.

IV. DISCUSSION

Given that the RPd_3S_4 compound series exists for most, if not all of the trivalent rare earths (R) and yttrium¹⁻⁴, but not, apparently, for the divalent alkaline earths, it is remarkable that $EuPd_3S_4$ not only accommodates such a large fraction of divalent europium, but that the fraction of Eu^{2+} is so robust against substitution by other trivalent rare earths: Substituting yttrium actually promotes the divalent state, whereas substituting lanthanum has little impact on the europium valence until at least half of the europium has been replaced.

It is clear that band filling or average valence electron count does not control the $Eu^{2+}:Eu^{3+}$ ratio in $R_xEu_{1-x}Pd_3S_4$ as both yttrium and lanthanum are triva-

lent yet act on the $\text{Eu}^{2+}:\text{Eu}^{3+}$ ratio in opposite directions. Similarly, chemical pressure arguments fail as lattice compression using yttrium substitution favours the larger Eu^{2+} ion, and lattice expansion using lanthanum leads to more of the smaller Eu^{3+} ion – the reverse of what would be predicted.

We are left with preservation of the average rare-earth size as the dominant factor controlling the $\text{Eu}^{2+}:\text{Eu}^{3+}$ valence ratio. Since $r_{\text{ionic}}(\text{Y}^{3+})$ is both smaller than $r_{\text{ionic}}(\text{Eu}^{3+})$ and much smaller than $r_{\text{ionic}}(\text{Eu}^{2+})$, converting Eu^{3+} into the larger Eu^{2+} as yttrium is added acts to maintain the average rare-earth size. By the same token, $r_{\text{ionic}}(\text{La}^{3+})$ lies between those of Eu^{2+} and Eu^{3+} , so lanthanum substitution initially has very little effect on the $\text{Eu}^{2+}:\text{Eu}^{3+}$ ratio. Only after half of the europium has been replaced do we see a shift in the balance towards Eu^{3+} .

Hydrostatic pressure would provide a complementary window on how pure changes in volume affect the $\text{Eu}^{2+}:\text{Eu}^{3+}$ ratio, and synchrotron Mössbauer spectroscopy under pressure would be a useful extension of this study.

Remarkably, La-substitution also appears to reduce the barrier for electron hopping between the Eu^{2+} and Eu^{3+} ions in $\text{La}_x\text{Eu}_{1-x}\text{Pd}_3\text{S}_4$, and a temperature dependent intermediate valence component develops at progressively lower temperatures with increasing lanthanum content. Extrapolating the composition trend in the onset temperature leads to the prediction that electron hopping should start around 340 K in un-doped EuPd_3S_4 . The much weaker dynamic behaviour in the Y-substituted series may reflect a stronger bias towards Eu^{2+} in $\text{Y}_x\text{Eu}_{1-x}\text{Pd}_3\text{S}_4$ which may in turn stabilise the valence of the two europium components. Alternatively, the much lower availability of Eu^{3+} for electron exchange may be the limiting factor.

The evolution of low temperature magnetism, as seen by Mössbauer spectroscopy, heat capacity and low field magnetic susceptibility also differs between yttrium and lanthanum. Remarkably, suppression of the ordering by the dilution of the magnetic Eu^{2+} is not the primary impact in either series. Magnetic order persists in $\text{Y}_x\text{Eu}_{1-x}\text{Pd}_3\text{S}_4$ even as far as $x=0.875$, with the onset temperature essentially unchanged, despite only about 12% of the europium sites being occupied by a moment-bearing ion (Fig. 17). However the behaviour of the La-substituted series is perhaps more surprising. Not only does the magnetic order also persist to $x=0.875$ (where the moment-bearing fraction is only $\sim 4\%$ because of the much lower $\text{Eu}^{2+}:\text{Eu}^{3+}$ ratio in the La-substituted series), but the onset temperature jumps from ~ 3 K to ~ 6 K for low x and remains near 6 K at least as far as $x=0.875$ (Fig. 17). We emphasise that our data do not provide access to the specific magnetic structures of the Y- and La- substituted materials. The behaviour of $\chi(T)$ and $C_p(T)$ in Fig. 5 strongly suggests that the parent compound orders antiferromagnetically, however it is unlikely that this survives the substitutional disorder in-

troducted when we replace the europium. The form of $\chi(T)$ clearly changes in both series (Figs. A.2 and A.4 in the appendix) and the magnetic order appears to develop at least some ferromagnetic character, although it is probably dominated by short ranged order. The extremely broad hyperfine field distributions and the presence of significant zero field components well below the onset of magnetic order in both $\text{La}_{0.25}\text{Eu}_{0.75}\text{Pd}_3\text{S}_4$ and $\text{Y}_{0.25}\text{Eu}_{0.75}\text{Pd}_3\text{S}_4$ (Fig. A.9) point to inhomogeneous ordering in both of these magnetically diluted materials.

V. CONCLUSIONS

The impact of yttrium and lanthanum substitution on mixed-valence EuPd_3S_4 has been studied using ^{151}Eu Mössbauer spectroscopy, bulk magnetisation and heat capacity measurements. Average valence electron count clearly does not control the europium valence distribution as trivalent yttrium and lanthanum substitutions have opposite effects. Similarly, chemical pressure arguments fail as lattice compression using yttrium substitution favours the larger Eu^{2+} ion, with the reverse effect seen with lanthanum. It appears that preservation of the average rare-earth size is the dominant factor controlling the $\text{Eu}^{2+}:\text{Eu}^{3+}$ valence ratio.

Lanthanum substitution was also found to promote electron hopping between the Eu^{2+} and Eu^{3+} ions, leading to the formation of intermediate valence europium. Increasing lanthanum substitution both increases the amount of intermediate valence europium seen at ambient temperatures and reduces the temperature at which hopping starts to appear. An onset temperature of ~ 340 K is predicted for undoped EuPd_3S_4 .

Inhomogeneous magnetic order is seen at all levels of substitution, with the onset temperature in the Y-substituted series being essentially unchanged at 3 K, while for the La-substituted series the onset temperature is seen to increase to 6 K despite the low concentration of magnetic ions.

ACKNOWLEDGMENTS

Financial support for this work was provided by Fonds Québécois de la Recherche sur la Nature et les Technologies, and the Natural Sciences and Engineering Research Council (NSERC) Canada.

Work at the Ames Laboratory was supported by the U.S. Department of Energy, Office of Science, Basic Energy Sciences, Materials Sciences and Engineering Division. The Ames Laboratory is operated for the U.S. Department of Energy by Iowa State University under contract No. DE-AC02-07CH11358.

BK is supported by the Center for the Advancement of Topological Semimetals (CATS), an Energy Frontier Research Center funded by the US DOE, Office of Basic Energy Sciences.

Much of this work was carried out while DHR was on

sabbatical at Iowa State University and their generous support during this visit is gratefully acknowledged.

- ¹ D. A. Keszler, J. A. Ibers, and M. H. Mueller, *J. Chem. Soc., Dalton Trans.*, 2369 (1985).
- ² M. Wakeshima, T. Fujino, N. Sato, K. Yamada, and H. Masuda, *Journal of Solid State Chemistry* **129**, 1 (1997).
- ³ M. Wakeshima and Y. Hinatsu, *Journal of Solid State Chemistry* **146**, 226 (1999).
- ⁴ P. Bonville, C. Godart, E. Alleno, F. Takahashi, E. Matsuoka, and M. Ishikawa, *Journal of Physics: Condensed Matter* **15**, L263 (2003).
- ⁵ M. Wakeshima, Y. Doi, Y. Hinatsu, and N. Masaki, *Journal of Solid State Chemistry* **157**, 117 (2001).
- ⁶ A. C. Larson and R. B. Von Dreele, Los Alamos National Laboratory Report LAUR 86-748 (2000).
- ⁷ B. H. Toby, *J. Appl. Cryst.* **34**, 210 (2001).
- ⁸ C. J. Voyer and D. H. Ryan, *Hyperfine Interact.* **170**, 91 (2006).
- ⁹ K. Abe, J. Kitagawa, N. Takeda, and M. Ishikawa, *Phys. Rev. Lett.* **83**, 5366 (1999).
- ¹⁰ E. R. Bauminger, D. Froindlich, I. Nowik, S. Ofer, I. Felner, and I. Mayer, *Phys. Rev. Lett.* **30**, 1053 (1973).
- ¹¹ A. Palenzona, S. Cirafici, and F. Canepa, *J. Less Common Met.* **119**, 199 (1986).
- ¹² M. M. Abd-Elmeguid, C. Sauer, and W. Zinn, *J. Phys. C: Solid State Phys.* **18**, 345 (1985).
- ¹³ J. Röhler, D. Wohlleben, G. Kaindl, and H. Balster, *Phys. Rev. Lett.* **49**, 65 (1982).
- ¹⁴ Z. Hossain, C. Geibel, N. Senthilkumaran, M. Deppe, M. Baenitz, F. Schiller, and S. L. Molodtsov, *Phys. Rev. B* **69**, 014422 (2004).

Appendix A: Additional figures and tables

This appendix contains additional figures showing heat capacity and susceptibility data for $Y_xEu_{1-x}Pd_3S_4$ and $La_xEu_{1-x}Pd_3S_4$.

We also present low temperature ^{151}Eu Mössbauer data for $La_{0.5}Eu_{0.5}Pd_3S_4$ showing the onset of magnetic broadening near 6 K, and spectra for $La_{0.25}Eu_{0.75}Pd_3S_4$ showing the inhomogeneous magnetic order that develops below the transition temperature. The temperature dependence of some fitting parameters for the $La_{0.25}Eu_{0.75}Pd_3S_4$ spectra is also shown.

The fitted lattice parameters and Eu^{2+} fractions used

to construct Fig. 6 in the main body of the text are also tabulated here.

x	a (Å)	Eu ²⁺ fraction (%)		
		Mössbauer	Curie-Weiss ±5%	M(H) ±5%
0.00	6.67858(8)	53.8(5)	57	49
0.125	6.67637(9)	56.3(8)	59	56
0.25	6.67371(13)	61.5(5)	66	63
0.375	6.66983(12)	68.4(5)	72	68
0.500	6.66527(20)	73.3(9)	71	69
0.625	6.66148(10)	83.2(7)	92	89
0.750	6.65514(12)	87.3(8)	85	86
0.875	6.64921(11)	93(2)	95	94
1.00	6.64193(17)	–	–	–

TABLE A.1. Measured lattice parameters and Eu^{2+} fractions for the $Y_xEu_{1-x}Pd_3S_4$ compound series.

x	a (Å)	Eu ²⁺ fraction (%)		
		Mössbauer	Curie-Weiss ±5%	M(H) ±5%
0.00	6.67858(8)	53.8(5)	57	49
0.25	6.69217(18)	53.1(6)	55	52
0.375	6.70125(17)	51.1(9)	53	49
0.50	6.70871(17)	51.5(8)	54	49
0.625	6.71763(12)	47(2)	53	46
0.75	6.72490(14)	46(2)	56	43
0.8125	6.72981(12)	39(1)	57	40
0.875	6.73316(14)	32(1)	61	36
0.9375	6.73557(6)	25(3)	86	34
1.00	6.73948(9)	–	–	–

TABLE A.2. Measured lattice parameters and Eu^{2+} fractions for the $La_xEu_{1-x}Pd_3S_4$ compound series.

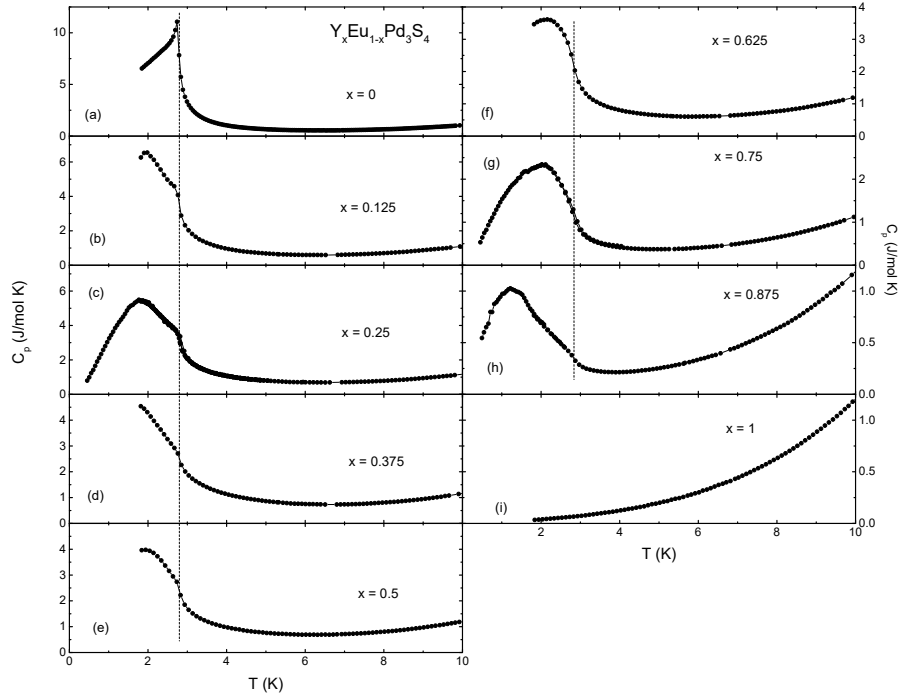


FIG. A.1. Heat capacity measurements for $Y_xEu_{1-x}Pd_3S_4$ showing the persistence of the magnetic transition near 3 K despite the significant dilution of the magnetic Eu^{2+} . At $x=1$ there is no transition observed as the system contains no magnetic species and so is paramagnetic. The vertical dashed lines mark 3 K.

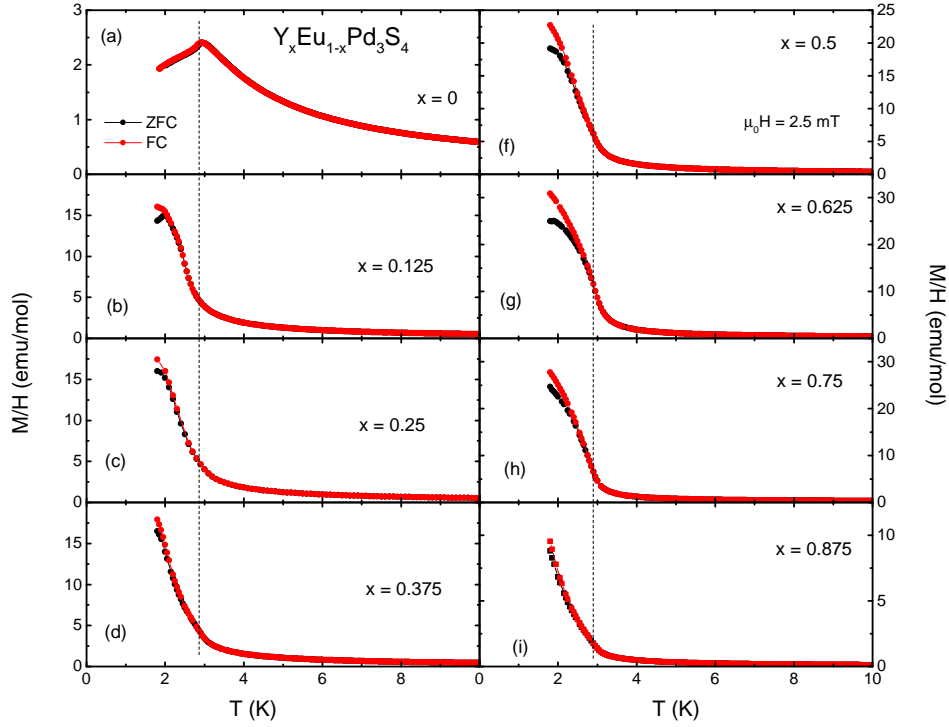


FIG. A.2. Field-cooled (FC) and zero-field-cooled (ZFC) dc susceptibility for $Y_xEu_{1-x}Pd_3S_4$ confirming the persistence of the magnetic transition seen near 3 K in the heat capacity data (Fig. A.1) despite the significant dilution of the magnetic Eu^{2+} . The vertical dashed lines mark 3 K.

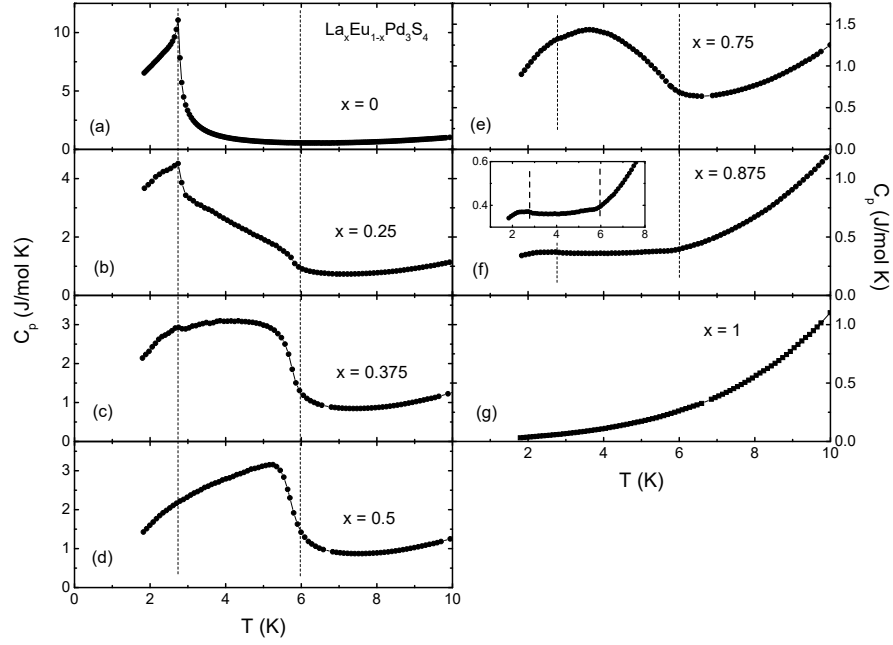


FIG. A.3. Heat capacity measurements for $\text{La}_x\text{Eu}_{1-x}\text{Pd}_3\text{S}_4$ showing the gradual replacement of the 3 K transition by a new feature at 6 K, despite the significant dilution of the magnetic Eu^{2+} component. The inset in (f) shows the region between 2 K and 8 K on an expanded vertical scale. At $x=1$ there is no transition observed as the system contains no magnetic species and so is paramagnetic. The vertical dashed lines mark 3 K and 6 K.

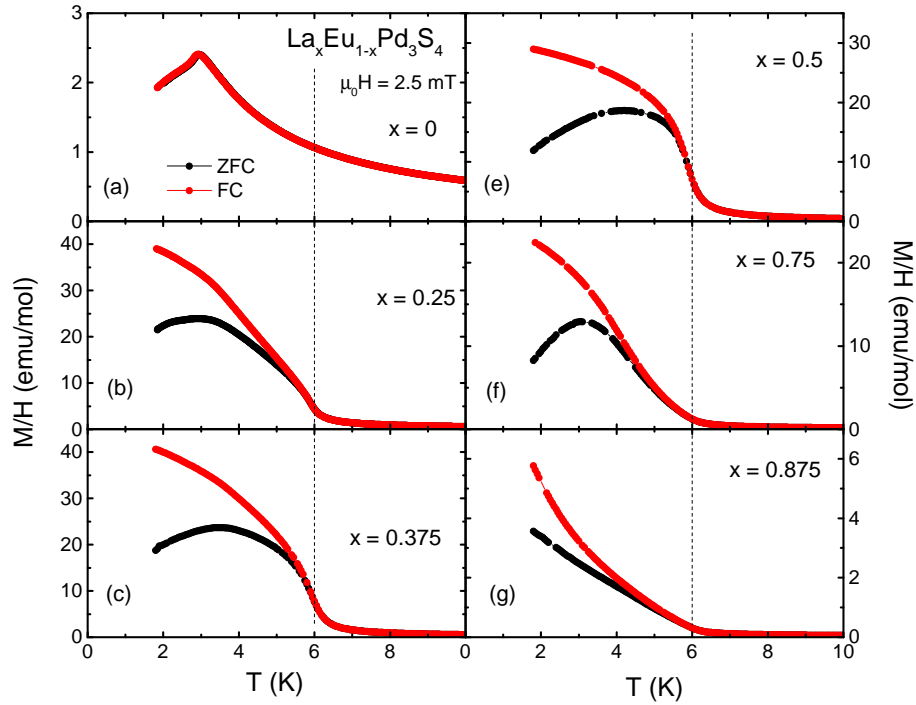


FIG. A.4. Field-cooled (FC) and zero-field-cooled (ZFC) dc susceptibility for $\text{La}_x\text{Eu}_{1-x}\text{Pd}_3\text{S}_4$ confirming the gradual replacement of the 3 K transition by a new feature at 6 K, seen in the heat capacity data (Fig. A.3) despite the significant dilution of the magnetic Eu^{2+} . The vertical dashed lines mark 3 K.

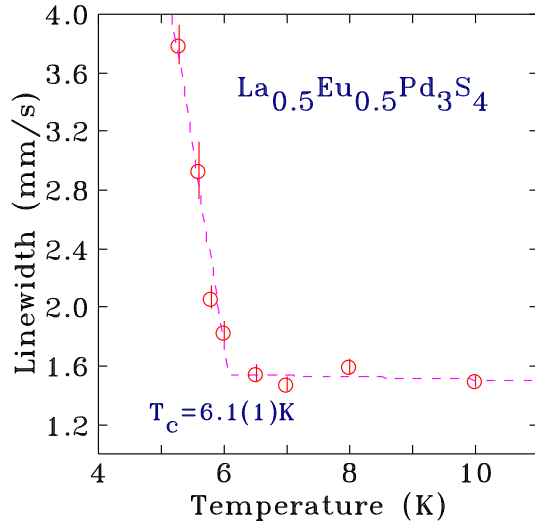


FIG. A.5. Temperature dependence of the Eu^{2+} line width in $\text{La}_{0.5}\text{Eu}_{0.5}\text{Pd}_3\text{S}_4$ showing the onset of ordering at 6.1(1) K.

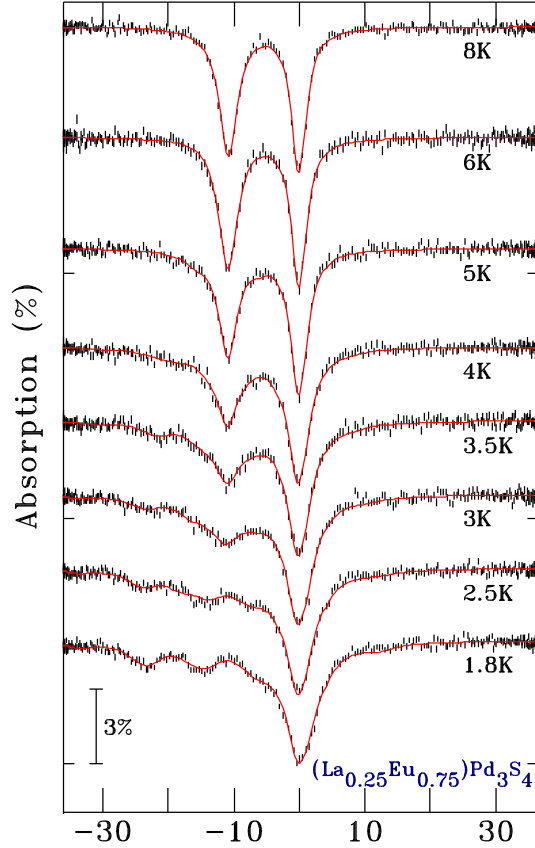


FIG. A.6. ^{151}Eu Mössbauer spectra of $(\text{La}_{0.25}\text{Eu}_{0.75})\text{Pd}_3\text{S}_4$ showing the progressive development of magnetic order in the Eu^{2+} component. The solid lines are fits using a single line for the Eu^{3+} line near 0 mm/s, and three components to fit the Eu^{2+} : an unsplit line, and two magnetic contributions with a “small” and “large” field used to reproduce the gross behaviour of the system.

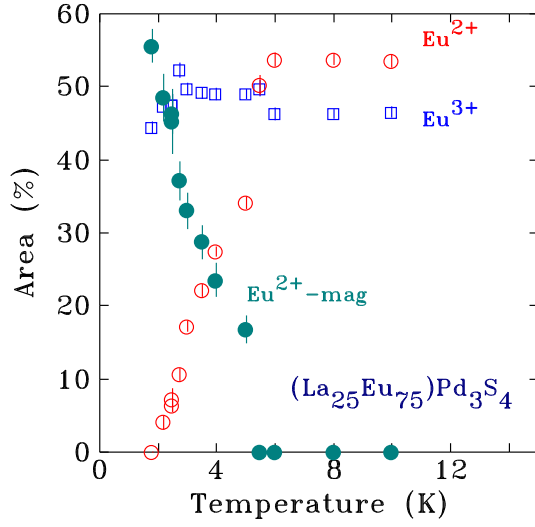


FIG. A.7. Temperature dependence of the magnetic and non-magnetic Eu^{2+} components in the ^{151}Eu Mössbauer spectra of $\text{La}_{0.25}\text{Eu}_{0.75}\text{Pd}_3\text{S}_4$ showing the gradual onset of magnetic order below 6 K but no evidence for a break at 3 K that might suggest the presence of a second phase.

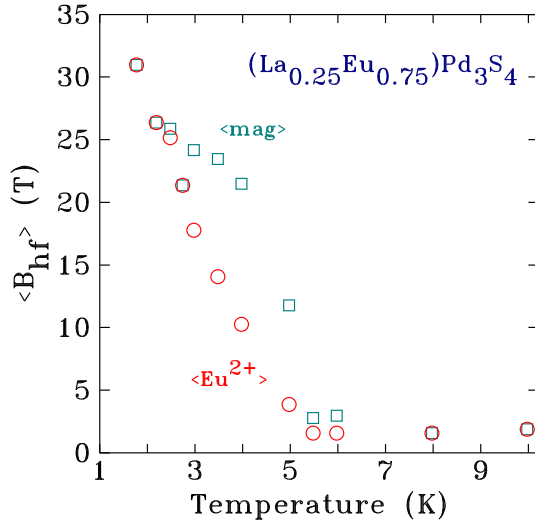


FIG. A.8. Temperature dependence of the average Eu^{2+} magnetic hyperfine field (B_{hf}) in the ^{151}Eu Mössbauer spectra of $\text{La}_{0.25}\text{Eu}_{0.75}\text{Pd}_3\text{S}_4$ showing the gradual onset of magnetic order below 6 K. Two averages are shown: (i) $\langle \text{Eu}^{2+} \rangle$ (blue circles) is calculated for all three Eu^{2+} components used in the fits; (ii) $\langle \text{mag} \rangle$ (red squares) is calculated omitting the Eu^{2+} component that exhibits no magnetic splitting. See text for details of the model used to fit the spectra.

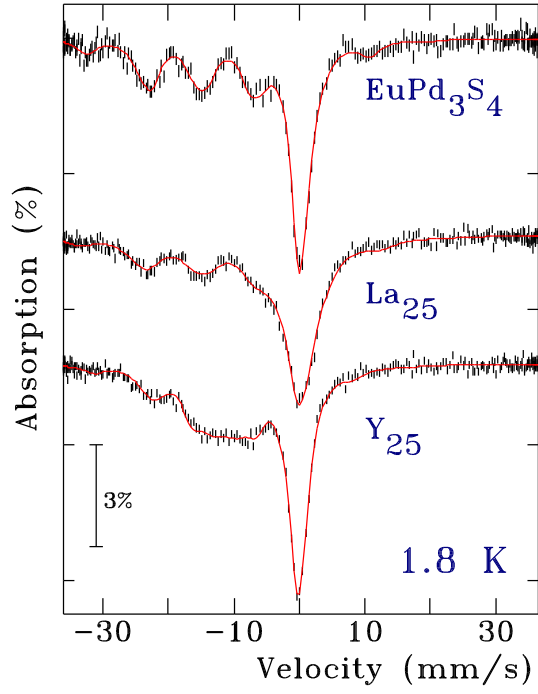


FIG. A.9. ^{151}Eu Mössbauer spectra of EuPd_3S_4 (top), $\text{La}_{0.25}\text{Eu}_{0.75}\text{Pd}_3\text{S}_4$ (middle) and $\text{Y}_{0.25}\text{Eu}_{0.75}\text{Pd}_3\text{S}_4$ (bottom) measured at 1.8 K showing that while the substituted materials do appear to exhibit magnetic ordering of the Eu^{2+} component, the lines are not sharp, reflecting a broad distribution of hyperfine fields.